J|A|C|S COMMUNICATIONS

Published on Web 07/20/2009

Anisotropic Growth of One-Dimensional Silver Rod−Needle and Plate−Belt Heteronanostructures Induced by Twins and hcp Phase

Xiao Shuang Shen, Guan Zhong Wang,* Xun Hong, Xing Xie, Wei Zhu, and Da Peng Li

Hefei National Laboratory for Physical Sciences at Microscale and Department of Physics, University of Science and Technology of China, Hefei, Anhui 230026, P. R. China

Received April 27, 2009; E-mail: gzwang@ustc.edu.cn

Heteronanostructures, which are nanosized single structures consisting of more than one component, can possess multiple properties simultaneously.[1] Since noble-metal nanostructures exhibit shape- and size-dependent properties,[2] single-component noble-metal nanostructures with one or more domains of different shapes or sizes epitaxially extended can be categorized as another type of heteronanostructure. In this regard, Klajn et al.[3] reported the synthesis of heterodimeric sphere−prism nanostructures via metastable gold supraspheres. In addition, Chen et al.[4] reported the fabrication of Au rod−sheath heteronanostructures that exhibit a significant electromagnetic enhancement at the junction of the rod and sheath. Here we report a one-step, high-yield synthesis of one-dimensional (1D) Ag heteronanostructures in aqueous solution. Besides the usual fcc phase of Ag, the heteronanostructures also contain a rare hcp (4H polytypic) phase, which favors the asymmetrical growth. We have found the variance of crystal structures in different segments of the heteronanostructures to be correlated with the formation process of such novel nanostructures.

In a typical synthesis, 10 mL of 25 mM sodium dodecyl sulfate (SDS) and 5 mM $AgNO_3$ aqueous solution was put in a 50 °C water bath under magnetic stirring. After 5 min, 5 mL of 5 mM ascorbic acid (AA) aqueous solution was added rapidly. The solution was allowed to react for 5 min at 50 °C, after which the products were collected by centrifugation.

Figure 1a provides a scanning electron microscopy (SEM) image of the sample, which shows that the products are 1D nanostructures with two distinct segments. One segment is rod-shaped with a hexagonal cross section (Figure 1a inset), and the other is needle-shaped with a gradually decreasing diameter. The ratio ($r_{N/R}$) of the needle and rod lengths is between 1 and 1.5. The products can be called rod−needle heteronanostructures (RNHSs). Figure 1b (also see Figure S1 in the Supporting Information) shows the X-ray diffraction (XRD) pattern of the RNHSs. Besides the typical peaks of fcc Ag, a peak also appears at ∼35.9°, which can be indexed to 4H Ag.[5]

Figure 1c is a transmission electron microscopy (TEM) image of a single RNHS, and the electron diffraction (ED) patterns taken from the needle and rod segments are shown in Figure 1d,e, respectively. According to the TEM image and ED patterns, the RNHS contains (111)/[112]-type growth twins,[6] and the growth direction is along the <111> direction. These results were further confirmed by high-resolution TEM (HRTEM) observations (Figure 1f). In addition, the presence of weak spots between the main spots in Figure 1d,e indicates that the needle segment has more (111) stacking faults than the rod segment. This is probably the reason that the needle segment is not as straight as the rod segment. In the needle segment, the HRTEM image also shows the existence of local 4H phases and other stacking faults (Figure 1g). The crystal structure of RNHSs is very similar to that of Ag nanorices obtained by Liang and co-workers[7] through a polyol process. Continuous

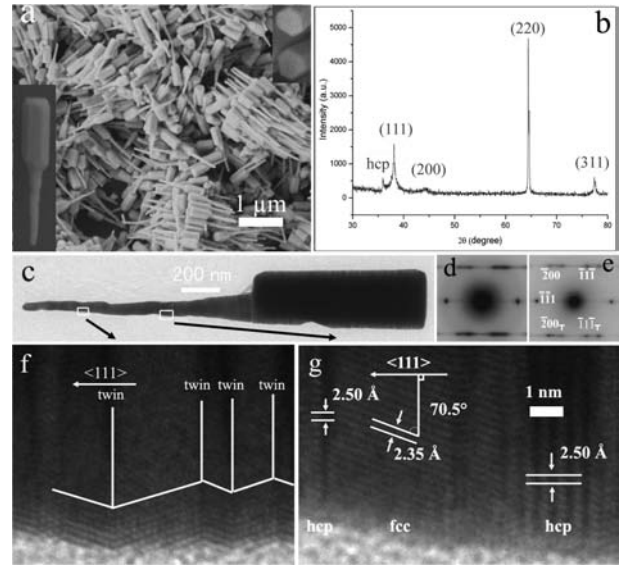

Figure 1. (a) SEM image of the rod−needle heteronanostructures (RNHSs) obtained with 5 mM AA and 5 mM $AgNO_3$. The lower-left inset is an enlarged SEM image of a single RNHS. The upper-right inset shows that the rods have hexagonal cross sections. (b) XRD pattern of the RNHSs. (c) TEM image of a single RNHS. (d, e) ED patterns taken from the needle and rod segments, respectively. (f, g) HRTEM images taken from the square-enclosed regions in (c).

formation of (111) twins, local 4H phases, and other stacking faults along one direction breaks the crystal symmetry of fcc Ag. This demonstrates an alternative mechanism for formation of 1D Ag nanostructures.

To reveal the growth process of the RNHSs, we took products with a short reaction time of 15 s. As shown in Figure 2a, the products are needle-shaped without an abrupt change in diameter along the long axis. In the sample shown in Figure 1a, an RNHS with a broken rod segment was imaged (Figure 2b), showing that the rod segment is formed through growth around the needle segment. According to these observations, we suggest the growth process of the RNHSs shown in Figure 2c. At the early stage, growth along the long axis leads to the formation of needles. Next, growth along the short axis causes the formation of rods around the thicker parts of the needles. We believe the high occurrence ratio of local 4H phases and other stacking faults in the thinner parts of the needles inhibits the growth along the short axis, which leads to the formation of RNHSs rather than rods. Control experiments conducted at 40 and 60 °C also support this formation mechanism (Figure S2).

The $r_{N/R}$ for the RNHSs could be controlled by changing the concentration of AA or $AgNO_3$. For example, when the concentration of AA was doubled while the other experimental conditions

10.1021/ja903389s CCC: $40.75

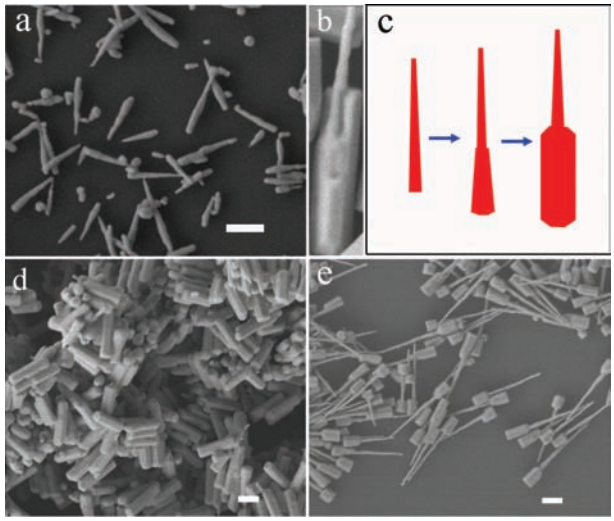

Figure 2. (a) SEM image of the sample with a short reaction time of 15 s. (b) SEM image of an RNHS with a broken rod segment. (c) Scheme illustrating the formation process of the RNHSs. (d, e) SEM images of the samples obtained with (d) 10 mM AA and 5 mM $AgNO_3$ and (e) 5 mM AA and 2.5 mM $AgNO_3$. All of the scale bars represent 500 nm.

remained the same, Ag nanorods (i.e., $r_{N/R} = 0$) accompanied by a few RNHSs with small $r_{N/R}$ (<0.5) were obtained (Figure 2d). It is worth pointing out that the 4H peak in the XRD pattern of this sample was very weak (Figure S3), which is consistent with the formation mechanism of the RNHSs we suggested above. On the other hand, RNHSs with large $r_{N/R}$ (between 2.5 and 4) were obtained when the concentration of $AgNO_3$ was cut in half to 2.5 mM (Figure 2e). The RNHSs were up to several micrometers in length.

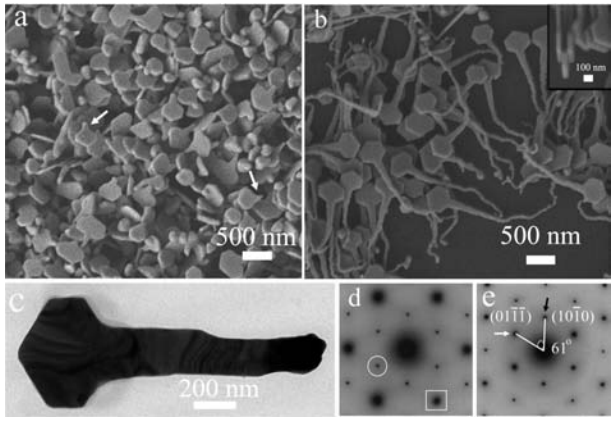

Figure 3. SEM images of the samples obtained with (a) 5 mM AA and 1.25 mM $AgNO_3$ and (b) 2.5 mM AA and 1.25 mM $AgNO_3$. The inset shows that the thickness of the plates was ~30−70 nm. (c) TEM image of a single plate−belt heteronanostructure (PBHS). (d, e) ED patterns taken from the plate and belt segments, respectively, of a PBHS.

When the concentration of $AgNO_3$ was further decreased to 1.25 mM, irregular hexagonal plates were obtained (Figure 3a). Interestingly, most of the plates had a tip on one of their corners (shown by arrows in Figure 3a). When the concentration of $AgNO_3$ was kept at 1.25 mM and the concentration of AA was decreased to 2.5 mM, regular hexagonal plates with belt-shaped tails were obtained (Figure 3b). These tadpole-like products can be called plate−belt heteronanostructures (PBHSs). The PBHSs had thicknesses of ~30−70 nm (Figure 3b inset) and lengths of several micrometers.

Figure 3c shows a TEM image of a single PBHS. The ED pattern taken from the plate segment of the PBHS is shown in Figure 3d. As for usual Ag plates, the spots enclosed by the square and circle could be assigned to the {220} and forbidden 1/3{422} reflections, respectively. The latter indicates the presence of twin planes in the {111} plane perpendicular to the electron beam.[8] These twin planes are thought to be responsible for the formation of Ag plates.[9] Figure 3e (also see Figure S4) shows the ED pattern taken from the belt segment of the PBHS. The spots marked with white and black arrows correspond to crystal planes with spacings of 2.43 and 2.51 Å, respectively. In addition, the angle between the reciprocal vectors of the two spots is 61°. According to the values of the spacings and the angle, the two spots can be assigned to (01$\bar{1}\bar{1}$) and (10$\bar{1}$0) of 4H Ag,[10] not fcc Ag. Thus, the zone axis of this electron diffraction pattern is [$\bar{1}$2$\bar{1}$3]. The HRTEM image further confirmed that the belt segment has a 4H structure (Figure S5). We also took the ED pattern from the plate−belt junction of the PBHS (Figure S6), which can be looked as the superposition of the spots shown in Figure 3d,e. The plate and belt segments indeed have different crystal structures. Huang et al.[11] recently reported the synthesis (via surfactant-assisted galvanic reductions) of belt-like Ag particles, which also have a 4H structure. Further studies are needed to reveal the relationship between the belt-like morphology and the 4H structure.

In summary, this work demonstrates that we can fabricate 1D Ag RNHSs and PBHSs, which are formed through two different mechanisms. For RNHSs, the 4H and fcc phases coexist but have different densities in different segments, while for PBHSs, the fcc and 4H crystal structures exist in the plate and belt segments respectively. Condition-sensitive coexisting phase preferences can be applied as a new way of controlling the shape and thus the properties of Ag nanostructures.

Acknowledgment. This work was supported by the Natural Science Foundation of China (Grants 10574122, 50772110, 50721091), the National Basic Research Program of China (2006CB922000, 2007CB925202, 2009CB939901), and KJCX2. YW.W06-3 of CAS.

Supporting Information Available: Experimental details, XRD and ED patterns, and HRTEM and SEM images of the samples prepared under different conditions. This material is available free of charge via the Internet at http://pubs.acs.org.

References

(1) (a) Hurst, S. J.; Payne, E. K.; Qin, L.; Mirkin, C. A. *Angew. Chem., Int. Ed.* **2006**, *45*, 2672. (b) Mieszawska, A. J.; Jalilian, R.; Sumanasekera, G. U.; Zamborini, F. P. *Small* **2007**, *3*, 722.
(2) (a) Tao, A. R.; Habas, S.; Yang, P. *Small* **2008**, *4*, 310. (b) Xia, Y.; Xiong, Y.; Lim, B.; Skrabalak, S. E. *Angew. Chem., Int. Ed.* **2009**, *48*, 60.
(3) Klajn, R.; Pinchuk, A. O.; Schatz, G. C.; Grzybowski, B. A. *Angew. Chem., Int. Ed.* **2007**, *46*, 8363.
(4) Chen, X.; Li, S.; Xue, C.; Banholzer, M. J.; Chartz, G. C.; Mirkin, C. A. *ACS Nano* **2009**, *3*, 87.
(5) (a) Novgorodova, D.; Gorshkov, A.; Mokhov, A. *Zap. Vseross. Mineral. Ova.* **1979**, *108*, 552. (b) Rocha, T. C. R.; Zanchet, D. *J. Phys. Chem. C* **2007**, *111*, 6989.
(6) Wang, B.; Fei, G. T.; Zhou, Y.; Wu, B.; Zhu, X.; Zhang, L. *Cryst. Growth Des.* **2008**, *8*, 3073.
(7) Liang, H.; Yang, H.; Wang, W.; Li, J.; Xu, H. *J. Am. Chem. Soc.* **2009**, *131*, 6068.
(8) (a) Pastoriza-Santos, I.; Liz-Marzán, L. M. *J. Mater. Chem.* **2008**, *18*, 1724. (b) Xiong, Y.; Siekkinen, A. R.; Wang, J.; Yin, Y.; Kim, M. J.; Xia, Y. *J. Mater. Chem.* **2007**, *17*, 2600.
(9) Lofton, C.; Sigmund, W. *Adv. Funct. Mater.* **2005**, *15*, 1197.
(10) Liu, X.; Luo, J.; Zhu, J. *Nano Lett.* **2006**, *6*, 408.
(11) Huang, T.-K.; Cheng, T.-H.; Yen, M.-Y.; Hsiao, W.-H.; Wang, L.-S.; Chen, F.-R.; Kai, J.-J.; Lee, C.-Y.; Chiu, H.-T. *Langmuir* **2007**, *23*, 5722.

JA903389S